JAERI-M
85-031

ANALYSIS OF TIME-OF-FLIGHT EXPERIMENT ON LITHIUM-OXIDE ASSEMBLIES BY A TWO-DIMENSIONAL TRANSPORT CODE DOT3.5

March 1985

Yukio OYAMA, Seiya YAMAGUCHI and Hiroshi MAEKAWA

日 本 原 子 力 研 究 所
Japan Atomic Energy Research Institute

JAERI-M レポートは，日本原子力研究所が不定期に公刊している研究報告書です。
入手の問合わせは，日本原子力研究所技術情報部情報資料課（〒319-11茨城県那珂郡東海村）あて，お申しこしください。なお，このほかに財団法人原子力弘済会資料センター（〒319-11 茨城県那珂郡東海村日本原子力研究所内）で複写による実費頒布をおこなっております。

JAERI-M reports are issued irregularly.
Inquiries about availability of the reports should be addressed to Information Division Department of Technical Information, Japan Atomic Energy Research Institute, Tokai-mura, Naka-gun, Ibaraki-ken 319-11, Japan.

編集兼発行　日本原子力研究所
印　　刷　いばらき印刷㈱

Analysis of Time-of-Flight Experiment on Lithium-Oxide Assemblies by a Two-Dimensional Transport Code DOT3.5

Yukio OYAMA, Seiya YAMAGUCHI and Hiroshi MAEKAWA

Department of Reactor Engineering
Tokai Research Establishment, JAERI

(Received January 31, 1985)

Calculational analyses were made on the time-of-flight experiment of neutron leakage spectra from lithium-oxide slabs. The uncertainties in the calculation due to modelling were examined and it was estimated to be 1-2 %. The calculational results were compared with the experimental ones. The calculations were carried out by a two-dimensional transport code DOT3.5 using ENDF/B-4 nuclear data file. The comparison of energy-integrated fluxes in C/E from made it clear that the tendency of discrepancy between both results depended on the thickness of assembly and leaking angle. The discrepancy of C/E was about 40 % at the maximum. The effect due to the cross section change to a new data of $^7Li(n,n't)^4He$ was also examined.

This type of comparison is useful for the systematic assesments. From the comparison, it was suggested that the angular distribution of secondary neutron should be improved in the calculation, and the correct differential data of cross section are required.

Keywords: Lithium-Oxide, DOT3.5, TOF Experiment, Analysis, $^7Li(n,n't)^4He$, Calculational Model , Time-of-Flight Experiment, Two-dimensional Transport Code

2次元輸送計算コードDOT 3.5による酸化リチウム体系TOF実験の解析

日本原子力研究所東海研究所原子炉工学部
大山幸夫・山口誠哉・前川　洋

（1985年1月31日受理）

酸化リチウム平板体系からの漏洩中性子スペクトルを中性子飛行時間（TOF）法によって測定した実験についての計算解析をおこなった。モデル化による計算の不確かさを調べ，それが1～2％程度であると評価した。計算は核データファイルENDF／B－4を使い，2次元輸送計算コードDOT 3.5を用いておこなった。エネルギ積分したスペクトルの計算値と実験値との比（C／E）をとり，その傾向が体系の厚みと中性子の漏洩する角度とに系統的に依存していることを明らかにした。その不一致は最大40％であった。また，$^{7}Li(n, n't)^{4}He$ 反応の新しい評価値を採用した時の影響も調べた。

この種の比較は系統的評価に有用であることを示し，その結果から，2次中性子の角度分布は計算ではうまく再現できず，微分断面積の精度に問題のあることが示唆された。

Content

目　　　次

1. Introduction

In the nuclear design of a fusion reactor blanket, the reliablilty of nuclear data and calculational methods is essential to estimate tritium breeding ratio, nuclear heating and so on. It is necessary to plan the benchmark experiment that provides systematic and parametric data for testing the nuclear data and methods.

As an exepriment for this purpose, the angle-dependent neutron spectra leaking from lithium-oxide slabs were measured and they are reported separately.[1) The experimental configuration was selected to be suitable for a two-dimensional analysis. The measured spectra were well-defined in the limited small region on the rear surface of the assembly by using a long collimator and were obtained as absolute values.

In the present work, the calculational analyses were made on the experiment by the two-dimensional transport code DOT3.5.[2) At first, calculations were carried out to examine the uncertainties associated with modelling adopted in the calculation as a parametric survey. It is important to assess the uncertainties in the detailed comparison between the experiment and calculation. The comparison between the experimental and calculational results was carried out using a reference model. Finally, the effect caused by the cross section change of $^{7}Li(n,n't)^{4}He$ was examined by comparing the results calculated by using both data of ENDF/B-4 and that of P.G. Young's evaluation.[3)

A short description of the experiment is given in chapter 2. The details of the calculations including a calculational model are given in chapter 3. The calculated and measured neutron spectra are compared and discussed in chapter 4.

2. Experiment

The experiment was carried out using 15 Mev neutrons produced by the reactions of 350 keV deuterons with tritium atoms adsorbed in a titanium target. The leakage neutron spectra from lithium-oxide (Li_2O) slabs were measured over the energy range between 0.5 and 15 MeV by the time-of-flight (TOF) method using an NE213 liquid scintillator. The experimental details are described in the previous report.[1] The experimental configuration is shown in Figs. 2.1 and 2.2. The slabs were placed at the distance of 20 cm from the neutron source. The neutron detector could command an central of area of the rear surface, which was about 88 cm^2 in projection, throuth the collimator. The distance from the surface to the detector was about 7 m. The measured angles were 0, 12.2, 24.9, 41.8 and 66.8 degrees corresponding to the symmetrical S_{16} angular quadrature set.

The experimental assemblies were consisted of Li_2O blocks covered with a staimless steel jacket of 0.2 mm thickness and supported by thin walled aluminum square tubes. The thicknesses of assemblies were 5.06, 20.24 and 40.48 cm.

The measured angle-dependent neutron flux, which corresponds to an angular flux given by an S_n calculation, was defined by the following:

$$\Phi(r=0,z=20+\ell,\Omega,E_n) = \frac{C(E_n)}{\varepsilon(E_n)\cdot\Delta\Omega\cdot A_s\cdot S_n\cdot T(E_n)}$$

$$[\mathrm{n/sr/cm^2/unit\ lethargy/source\ neutron}]\ , \qquad (2.1)$$

where

$\Phi(r=0,z=20+\ell,\Omega,E_n)$: angular flux per unit area for the neutrons of energy E_n and angle Ω at $(r=0,z=20+\ell)$,

$C(E_n)$: counts per unit lethargy for the neutrons of energy E_n,

$\varepsilon(E_n)$: detector efficiency for the neutrons of energy E_n,

ℓ : thickness of the slab assembly,

Ω : solid angle subtended by the detector to a point on the surface of the assembly (A_d/L^2),

A_d : counting area of the detector,

L : neutron flight path,

A_s : effective measured area defined by the detector-collimator system on the plane perpendicular to the collimator axis at the assembly surface ($r=0$, $z=20+\ell$),

S_n : source neutron yield obtained by the alpha monitor,

$T(E_n)$: attenuation due to air in the flight path.

The source neutron spectrum used in this analysis was measured by the same TOF system. The spectrum is shown in Fig. 2.3 and given by the form:

$$\Phi_s(\Omega,E_n) = \frac{C(E_n)}{\varepsilon(E_n)\cdot\Delta\Omega\cdot S_n\cdot T(E_n)}$$

$$[\text{n/sr/unit lethargy/source neutron}]. \qquad (2.2)$$

The Eqs. 2.1 and 2.2 have the source neutron term S_n in common and thus the systematic error of S_n is cancelled.

The uncertainties of experiment are summarized in Table 2.1. These uncertainties are caused mainly by the determination of effective measured area and time zero.

3. Calculation

3.1 Calculational Procedure

In this analysis, a two-dimensional discrete ordinate transport code DOT3.5[2] was selected by the reason why it was widely used. The order of Legendre expansion on the cross section set and the angular quadrature set were adopted to be P_5 and S_{16}. A first collision source (FCS) method was applied to eliminate "Ray-effect".

The neutron group cross section sets were GICXFNS[4] and GICXFNS1 processed from the evaluated nuclear data files using the NJOY code.[5] In the GICXFNS1, the nuclear data in ENDF/B-4[6] were used for all nuclides. In the GICXFNS, for the nuclides other than ^{7}Li, the nuclear data in ENDF/B-4 were used. As for ^{7}Li, the nuclear data in ENDF/B-4 was used with the following modification. The ^{7}Li(n, n't)^{4}He reaction cross section in the original ENDF/B-4 was replaced by the one recently evaluated by P.G. Young.[3] In order to preserve the total cross section of ^{7}Li, the elastic cross section had also been changed to compensate for the change introduced by the replacement of the ^{7}Li(n, n't)^{4}He reaction.

To save the computer resources, the upper 68 group cross sections above 0.5 MeV are selected from the original 135 group cross sections. The group structure of GICXFNS is shown in Table 3.1. The interval of spatial mesh was determined to be 1 cm based on a calculational survey.

3.2 Calculational Model

In order to determine a calculational model, the following items were examined:

(1) Characteristics of neutron source, i.e., yield, angular distribution and energy spectrum,

(2) Effect of nonuniformity of atomic densities in the assembly and effect of aluminum lattice used to support the assembly,

(3) Treatment of the finite measured area in the calculation.

3.2.1 Neutron Source

As the angular flux obtained from the calculation is strongly dependent on the input neutrons, the source condition should be treated accurately. The following assumptions can be adopted from the results of the source characteristics measurement[1], since the measured angular fluxes depend mainly on the 15 MeV peak of source neutron spectrum.

1) Energy spectrum at any direction is the same as the spectrum obtained by the measurement in the zero degree direction to the incident deuteron beam.
2) Angular distribution of emitted neutron is isotropic over 4π direction, i.e., the source normalization factor in the calculation is the integration of the measured zero-degree angular flux multiplied by the whole solid angle 4π.

The d-D reaction neutrons were not included in the source neutrons to simplify the problem, because these neutrons depended on the irradiation history of the tritium target. This limitation gives the change less than a few % to the results for the lower energy region.

3.2.2 Assembly

The experimental assembly as built did not have a free boundary because of the existence of aluminum lattice for suppont. The atomic density was not uniform due to the usage of the various sizes of lithium-oxide blocks and the deviation of homogenized density was about 2 % between the central and outer regions. The densities of nuclides are shown in Table 3.2. The A type blocks were gathered to the central region. The assembly with the uniform density of A type and without Aluminum lattice were used as a reference assembly. The test calculations were carried out with and without aluminum lattice, and with uniform and nonuniform density for the 20.24 cm-thick assembly.

The angular flux was calculated by DOT3.5. The GRTUNCL code[2)] was adopted to calculate the first collision source for a multi-regional model as shown in Fig. 3.1. The results of calculations are summarized in Table 3.3. The deviation of angular fluxes caused by adopting the reference model without aluminum lattice and with uniform density was estimated to be within 1 %, excluding a few case. The effect of rectangular shape of the boundary was also examined by changing the radius of the assembly from 31.4 cm to 29.0 cm. This change was estimated to be within 1 % for the angular fluxes. Thus the simplified model as shown in Fig. 3.2 can be used for all cases.

3.2.3 Finite measured area

The measured angular flux was averaged over the effective measured area defined by the detector-collimator system. To average the angular flux over the measured area should be considered if the angular flux leaking from the lithium-oxide assembly does not have a uniform radial distribution. The radial distribution on the leakage surface of the assembly is dependent on anisotropy of scattering and r^{-2} law. The calculational distribution of angular flux for various direction with fixed polar angle and azimuthal angle ($\cos^{-1}\eta$, $\cos^{-1}\mu$) are given in Fig. 3.3 for the 20.24 cm-thick case. The radial distributions depend strongly on angle $\cos^{-1}\mu$. It is clear that radial averaging is necessary. The procedure of averaging is described as the following.

The angular flux on the central axis is symmetric with respect to the z axis. The other angular flux, however, is not symmetric and so the angular flux directed to the detector must be chosen among the angular fluxes with various azimuthal angles $\cos^{-1}\mu$. (See Fig. 3.4) As shown in Fig. 3.5 the average with respect to angle $\cos^{-1}\mu$ is equivalent to the average along a circle with a radius of r. The contribution of angular flux is also dependent on the radius r. Thus the calculational results are averaged with respect to the angle $\cos^{-1}\mu$ and the radius as follows:

$$<\Phi(\eta,r)>_{\mu} = \frac{\sum_{\mu}\omega_{\mu\eta}\Phi(\mu,\eta,r)}{\sum_{\mu}\omega_{\mu\eta}} \qquad (3.1)$$

$$<\Phi(\eta)>_{\mu,r} = \frac{\sum_{r}2\pi r\cdot<\Phi(\eta,r)>_{\mu}}{\sum_{r}2\pi r} , \qquad (3.2)$$

where

Φ : angular flux,

$\phi = \cos^{-1}\mu$: azimuthal angle,

$\theta = \cos^{-1}\eta$: polar angle,

$\omega_{\mu\eta}$: angular weight for S_{16} quadrature set,

r : radius of calculated point.

The radial averaging was carried out upto 5 cm in radius considering to the area defined by the collimator system. The ratios of the radial averaging flux to the angular flux on the central point (r=0) were examined for the energy integrated fluxes. This averaging effect was estimated to be about 5 % as shown in Fig. 3.6.

From the above discussions, the following assumptions were adopted on the calculation. The expected uncertainty caused by the assumptions was within 1-2 % to the calculational results.

1) Neutron source is isotropic.

2) Density of materials is uniform over the assembly.

3) Radius of assembly is given as the area-equivaent radius.

4) Angular flux is averaged over the effective measured area of 5 cm radius

4. Comparison with Experiment

This comparison was carried out for the spectral shape and integrated flux using GICXFNS1. The ratio of the calculation to the experimental values, C/E, is very useful for understanding the tendency. Finally two cross section sets of $^{7}Li(n, n't)^{4}He$, i.e., the one of ENDF/B-4 and the other evaluated recently by P.G. Young, were examined by applying them to this calculation.

The comparisons of the zero-degree data were excluded, since their data need the additional procedure, e.g., angle extrapolation due to lack of the angular mesh point and uncollided flux correction in order to extrapolate it to the detector position. The 12.2 degree data of the 5.06 cm-thick assembly was also excluded because the measured value had contamination of the uncollided flux.

4.1 Spectra

The comparison between the measured angle-dependent spectra and the calculated one are shown in Figs. 4.1 - 4.11 with the parameters of leaking angle and thickness of assembly. The observed angular spectra from Li_2O slabs are constructed of the peaks of scattered neutrons by lithium and oxygen, and valleys caused by resonance scatterings of oxygen. The energy within 1-2 % to the calculational results.

1) Neutron source is isotropic.

2) Density of materials is uniform over the assembly.

3) Radius of assembly is given as the area-equivaent radius.

4) Angular flux is averaged over the effective measured area of 5 cm radius

4. Comparison with Experiment

This comparison was carried out for the spectral shape and integrated flux using GICXFNS1. The ratio of the calculation to the experimental values, C/E, is very useful for understanding the tendency. Finally two cross section sets of $^{7}Li(n, n't)^{4}He$, i.e., the one of ENDF/B-4 and the other evaluated recently by P.G. Young, were examined by applying them to this calculation.

The comparisons of the zero-degree data were excluded, since their data need the additional procedure, e.g., angle extrapolation due to lack of the angular mesh point and uncollided flux correction in order to extrapolate it to the detector position. The 12.2 degree data of the 5.06 cm-thick assembly was also excluded because the measured value had contamination of the uncollided flux.

4.1 Spectra

The comparison between the measured angle-dependent spectra and the calculated one are shown in Figs. 4.1 - 4.11 with the parameters of leaking angle and thickness of assembly. The observed angular spectra from Li_2O slabs are constructed of the peaks of scattered neutrons by lithium and oxygen, and valleys caused by resonance scatterings of oxygen. The energy spectrum in the range from 11 to 15 MeV is determined by elastic scatterings of ^{16}O, ^{7}Li and ^{6}Li nuclei, in the range from 3 to 10 MeV by inelastic scatterings of ^{16}O nuclei and in the range from 8 to 11 MeV by inelastic scatterings of ^{7}Li nuclei. The valleys near the energy 1 MeV is caused by resonance scatterings of ^{16}O nuclei in penetrating the assembly.

The spectra calculated by DOT3.5 represents well these peaks except the peaks near 9 MeV. The discrepancy near 9 MeV is due to the lack of 4.63 MeV level of ^{7}Li in ENDF/B-4 nuclear data file. This discrepancy, however, becomes small as the angle and thickness of assembly increase. The calculated results at the energy below 5 MeV for the thick assembly shift to high energy side compared to the experimental ones. This shows that the observed lower energy neutrons have the uncertainty of energy scale more than higher energy neutrons as the valleys caused by the resonance scattering of oxygen should be at the energies of 1.0 and 1.3 MeV exactly. Better agreement would be obtained by correcting energy scale using this results for the detailed differential comparison.

4.2 Integrated Flux

Three energy groups of the measured spectra are selected to make the comparison between the experimental and calculational fluxes by means of C/E. Three groups represent the elastic, inelastic and continuum level scattering regions, respectively. The results are shown in Fig. 4.12. The error bars mean statistical errors and dotted lines show the range of systematic error in the experiment. It is clear from the results that the discrepancy depends on the thickness and angle. As the thickness and angle increase, the C/E ratios depart from unity. The calculated valus for large angles are overestimated about 40 % for the 40 cm-thick assembly. The calculated values in a region of 5-10 MeV are underestimated, but the dependence on the thickness and angle is similar to the other regions. This underestimstion is due to the lack of cross section data of 4.63 MeV level of ^{7}Li in ENDF/B-4.

The error of energy scale is +5 % for the 40 cm-thick assembly in the experiment. The energy scale of the experimental spectrum was shifted by +5 % and the deviation of C/E was examined. This effect, however, was relatively small compared to the discrepancy of C/E as shown in Table 4.1.

The angular dependence of C/E for each case seems to vary systematically as shown in Fig. 4.12. In the 5 cm-thick case, the calculated fluxes between 24.9 and 41.8 degrees are overestimated for the elastic region which has a large dependence on the emitted angle. Though the C/E for the large angles increases with the thickness, the forward fluxes agree well with the experimental ones. This fact suggests that the overestimation of secondary neutrons for the direction between 24.9 and 41.8 degrees causes the large discrepancy for the large angle in the 40.48 cm-thick assembly, since the angular flux for the large angle is made of the last collision source in the outer region of the assembly.

4.3 Effect of Cross Section Change of ^{7}Li

Young's evaluation gives a value of 10-15 % lower than ENDF/B-4 data for tritium production cross section. The elastic cross section was increased to conserve a total cross section in the cross section set. The effect of this change is examined on the leakage spectra. The comparison between the ENDF/B-4 and Young's evaluation is shown in Fig. 4.13. This effect enlarges as the thickness increases ,and is estimated to be a few % for the 40 cm-thick assembly. The discrepancy between the calculational and the exprimental results is improved in the energy region below 10 MeV by using Young's evaluation, while in the elastic energy region it becomes worse. This result seems to suggest the unappropriate change of elastic cross section of ^{7}Li.

5. Summary

Before starting the analysis of the TOF experiment on the lithium-oxide slabs, the limitation of the calculational model was examined by a calculational survey. It became clear that the simple model used in the present analysis made the uncertainty of 1-2 %. The neutron leakage spectra calculated by a two-dimensional transport code DOT3.5 were compared with the experimental ones. These results are summarized as the following.

1) The agreement between the calculated and measured spectra are very good considering the absolute comparison. The calculated spectra shapes express well the experimental ones except the peak due to 4.63 MeV level of ^{7}Li.

2) The comparison of fluxes integrated over an adequate energy region makes it clear that the tendency of discrepancy between both results depends on the thickness of assembly and leaking angle. This type of comparison is useful and important for the systematic assesments.

3) From the tendency of the integrated flux comparison, it was suggested that the angular distribution of secondary neutron should be improved in the calculation, and the correct differential data of cross sections are required.

4) The nuclear data set based on the Young's evaluation gives a little change to the calculated angular spectrum. This change is undesirable for the elastic energy region, but in the inelastic and continuum regions give a small improvement.

Acknowledgments

The authors thank Mr. Nakamura for his support and helpful advice to this work. They thank Drs. S. Tanaka, Y. Ikeda and M. Nakagawa for the valuable discussions. They also wish to thank Mr. Fukumoto for his comment based on his pre-analysis, and Dr. Y. Seki for the usage of GICXFNS cross section set and the helpful suggestions during the phases of this analysis.

References

1) Oyama Y., Maekawa H.:" Measurement of Angle-Dependent Neutron Spectra from Lithium-Oxide Slab Assemblies by Time-of-Flight Method, " JAERI-M 83-195 (1983)
2) Rhodes W.A. , Mynatt F.R.:" The DOT-III Two Dimensional Discrete Ordinates Transport Code, " ORNL/TM-4280 (1973)
3) Young P.G. : Trans. Am. Nucl. Soc., vol.39, 272 (1981)
4) Seki Y., et al.:" Calculation of Absolute Fission-Rate Ditributions Measured in Graphite-Reflected Lithium Oxide Blanket Assembly, " JAERI-M 83-061 (1983)
5) MacFarlane R.E., et al.: " The NJOY Nuclear Data Processing System: User's Mannual, " LA-7584-M (ENDF-272) (1978)
6) Drake M.K. (edited)," Data Formats and Procedures for the ENDF Neutron Cross Section Library, " BNL-50274 (T-601, TID-4500), ENDF 102, vol.1 (1970), Revised 1974

Acknowledgments

The authors thank Mr. Nakamura for his support and helpful advice to this work. They thank Drs. S. Tanaka, Y. Ikeda and M. Nakagawa for the valuable discussions. They also wish to thank Mr. Fukumoto for his comment based on his pre-analysis, and Dr. Y. Seki for the usage of GICXFNS cross section set and the helpful suggestions during the phases of this analysis.

References

1) Oyama Y., Maekawa H.:" Measurement of Angle-Dependent Neutron Spectra from Lithium-Oxide Slab Assemblies by Time-of-Flight Method, " JAERI-M 83-195 (1983)

2) Rhodes W.A. , Mynatt F.R.:" The DOT-III Two Dimensional Discrete Ordinates Transport Code, " ORNL/TM-4280 (1973)

3) Young P.G. : Trans. Am. Nucl. Soc., vol.39, 272 (1981)

4) Seki Y., et al.:" Calculation of Absolute Fission-Rate Ditributions Measured in Graphite-Reflected Lithium Oxide Blanket Assembly, " JAERI-M 83-061 (1983)

5) MacFarlane R.E., et al.: " The NJOY Nuclear Data Processing System: User's Mannual, " LA-7584-M (ENDF-272) (1978)

6) Drake M.K. (edited)," Data Formats and Procedures for the ENDF Neutron Cross Section Library, " BNL-50274 (T-601, TID-4500), ENDF 102, vol.1 (1970), Revised 1974

Table 2.1 Uncertainty of the experimental results

Energy Resolution

item	Assembly 5 cm	20 cm	40 cm
time resolution		± 2 %	
emission time spread	< ± 1 %	< ± 3 %	< ± 5 %

Energy Scale

item	Assembly 5 cm	20 cm	40 cm
time zero	< ± 1 %	< ± 3 %	< ± 5 %

Flux

item	random	systematic
S_n	< ±1 %	± 2.2 %
$\varepsilon(E_n)\cdot\Delta\Omega$	± 3 ∿ 5 %	< + 2 %
A_s	± 0.5 %	< ± 2 %
$C(E_n)$	± 1 ∿ 20 %	< + 1 %
$T(E_n)$		negligible
overall *	± 3 ∿ 20 %	-2 ∿ +5 %

* excluding the error due to the absolute source neutrons that is cancelled by using the experimental source in the calculation.

Table 3.1 135 group neutron energy group structure of GICXFNS

Group	Energy limits	Mid-point energy
1	16.399 - 16.110 MeV	16.2545 MeV
2	16.110 - 15.825	15.9675
3	15.825 - 15.545	15.6850
4	15.545 - 15.270	15.4075
5	15.270 - 15.000	15.1350
6	15.000 - 14.735	14.8675
7	14.735 - 14.474	14.6045
8	14.474 - 14.218	14.3460
9	14.218 - 13.967	14.0925
10	13.967 - 13.720	13.8435
11	13.720 - 13.477	13.5985
12	13.477 - 13.239	13.3580
13	13.239 - 13.005	13.1220
14	13.005 - 12.775	12.8900
15	12.775 - 12.549	12.6620
16	12.549 - 12.182	12.3655
17	12.182 - 11.825	12.0035
18	11.825 - 11.479	11.6520
19	11.479 - 11.143	11.3110
20	11.143 - 10.817	10.9800
21	10.817 - 10.500	10.6585
22	10.500 - 10.089	10.2945
23	10.089 - 9.693	9.8910
24	9.693 - 9.314	9.5035
25	9.314 - 8.949	9.1315
26	8.949 - 8.598	8.7735
27	8.598 - 8.261	8.4295
28	8.261 - 7.938	8.0995
29	7.938 - 7.627	7.7825
30	7.627 - 7.327	7.4770
31	7.327 - 7.041	7.1840
32	7.041 - 6.765	6.9030
33	6.765 - 6.500	6.6325
34	6.500 - 6.242	6.3710
35	6.242 - 5.995	6.1185
36	5.995 - 5.757	5.8760
37	5.757 - 5.529	5.6430
38	5.529 - 5.310	5.4195
39	5.310 - 5.099	5.2045
40	5.099 - 4.897	4.9980
41	4.897 - 4.707	4.8000
42	4.703 - 4.516	4.6095
43	4.516 - 4.337	4.4265
44	4.337 - 4.165	4.2510
45	4.165 - 4.000	4.0825

Table 3.1 Continued

Group	Energy limits	Mid-point energy
46	4.000 - 3.699 MeV	3.8495 MeV
47	3.699 - 3.419	3.5590
48	3.419 - 3.162	3.2905
49	3.162 - 2.924	3.0430
50	2.924 - 2.704	2.8140
51	2.704 - 2.500	2.6020
52	2.500 - 2.270	2.3850
53	2.270 - 2.061	2.1655
54	2.061 - 1.871	1.9660
55	1.871 - 1.698	1.7845
56	1.698 - 1.542	1.6200
57	1.542 - 1.400	1.4710
58	1.400 - 1.275	1.3375
59	1.275 - 1.162	1.2185
60	1.162 - 1.058	1.1100
61	1.058 - 0.964	1.0110
62	0.964 - 0.878	0.921
63	0.878 - 0.800	0.839
64	0.800 - 0.713	0.7565
65	0.713 - 0.635	0.6740
66	0.635 - 0.566	0.6005
67	0.566 - 0.504	0.5350
68	0.504 - 0.449	0.4765
69	0.449 - 0.400	0.4245
70	0.400 - 0.356	0.3780
71	0.356 - 0.317	0.3365
72	0.317 - 0.283	0.3000
73	0.283 - 0.252	0.2675
74	0.252 - 0.224	0.2380
75	0.224 - 0.200	0.2120
76	0.200 - 0.178	0.1890
77	0.178 - 0.159	0.1685
78	0.159 - 0.141	0.1500
79	0.141 - 0.126	0.1335
80	0.126 - 0.112	0.1190
81	0.112 - 0.100	0.1060
82	0.100 - 0.0774	0.0887
83	77.4 - 59.9 KeV	68.65 KeV
84	59.9 - 46.4	53.15
85	46.4 - 35.9	41.15
86	35.9 - 27.3	31.35
87	27.3 - 21.5	24.65
88	21.5 - 16.7	19.10
89	16.7 - 12.9	14.80
90	12.9 - 10.0	11.45

Table 3.1 Continued

Group	Energy limits	Mid-point energy
91	10.0 - 7.74 KeV	8.870 KeV
92	7.74 - 5.99	6.865
93	5.99 - 4.64	5.315
94	4.64 - 3.59	4.115
95	3.59 - 2.78	3.185
96	2.78 - 2.15	2.465
97	2.15 - 1.67	1.910
98	1.67 - 1.29	1.480
99	1.29 - 1.00	1.145
100	1.00 - 0.774	0.8870
101	0.774 - 0.599	0.6865
102	0.599 - 0.464	0.5315
103	0.464 - 0.359	0.4115
104	0.359 - 0.278	0.3185
105	0.278 - 0.215	0.2465
106	0.215 - 0.167	0.1910
107	0.167 - 0.129	0.1480
108	0.129 - 0.100	0.1145
109	0.100 - 0.0774	0.0887
110	77.4 - 59.9 eV	68.65 eV
111	59.9 - 46.4	53.15
112	46.4 - 35.9	41.15
113	35.9 - 27.8	31.85
114	27.8 - 21.5	24.65
115	21.5 - 16.7	19.10
116	16.7 - 12.9	14.80
117	12.9 - 10.0	11.45
118	10.0 - 7.74	8.870
119	7.74 - 5.99	6.865
120	5.99 - 4.64	5.315
121	4.64 - 3.59	4.115
122	3.59 - 2.78	3.185
123	2.78 - 2.15	2.465
124	2.15 - 1.67	1.910
125	1.67 - 1.29	1.480
126	1.29 - 1.00	1.145
127	1.00 - 0.774	0.8870
128	0.774 - 0.599	0.6865
129	0.599 - 0.464	0.5315
130	0.464 - 0.359	0.4115
131	0.359 - 0.278	0.3185
132	0.278 - 0.215	0.2465
133	0.215 - 0.167	0.1910
134	0.167 - 0.129	0.1480
135	0.129 - 0.010	0.0695

Table 3.2 Homogenized atomic densities of the composition of each region in the assembly

Region	Element Type*1	Atomic Density ($atoms/cm^3$) A	B	C
Li_2O	^6Li	4.274+21*2	4.194+21	4.046+21
	^7Li	5.343+22	5.244+22	5.058+22
	O	2.885+22	2.832+22	2.731+22
	Fe	1.079+21	1.199+21	1.448+21
	Ni	1.309+20	1.454+20	1.756+20
	Cr	2.993+20	3.325+20	4.016+20
	Mn	2.393+19	2.658+19	3.211+19
Support	Al		1.067+22	
	Mg		6.000+19	
	Si		4.354+19	
	Fe		1.145+19	

*1 type A: 50.6 x 50.6 x 203 , type B: 50.6 x 50.6 x 102 ,
type C: 50.6 x 50.6 x 50.6

*2 read as 4.274×10^{21}

*3 type A was used as reference assembly

Table 3.3 Deviation of the more realistic model from the simplified model for two energy groups

Relative ratios are shown in the tables
(Averaged angular flux)

(a) Non-uniformity effect of Li_2O assembly
(non-uniform/uniform)

	15.000-14.735 MeV	3.419-3.162 MeV
12.2°	0.9988	1.0012
24.9°	1.0002	0.9985
41.8°	1.0093	0.9981
66.8°	1.0158	0.9976

(b) Aluminum support effect
(with/without Aluminum support)

	15.000-14.735 MeV	3.419-3.162 MeV
12.2°	1.0000	0.9993
24.9°	1.0001	0.9988
41.8°	1.0025	0.9991
66.8°	1.0007	0.9987

Table 4.1 Effect of +5 % change in energy scale

Energy (MeV)	12.2°	24.9°	41.8°	66.8°
$10 < E_n$	0.992	0.971	0.948	0.910
$4.75 < E_n < 10$	1.015	1.031	1.032	1.053
$0.45 < E_n < 4.75$	1.014	1.015	1.014	1.005

$ 40 cm-thick assembly

* Ratio of C/E change

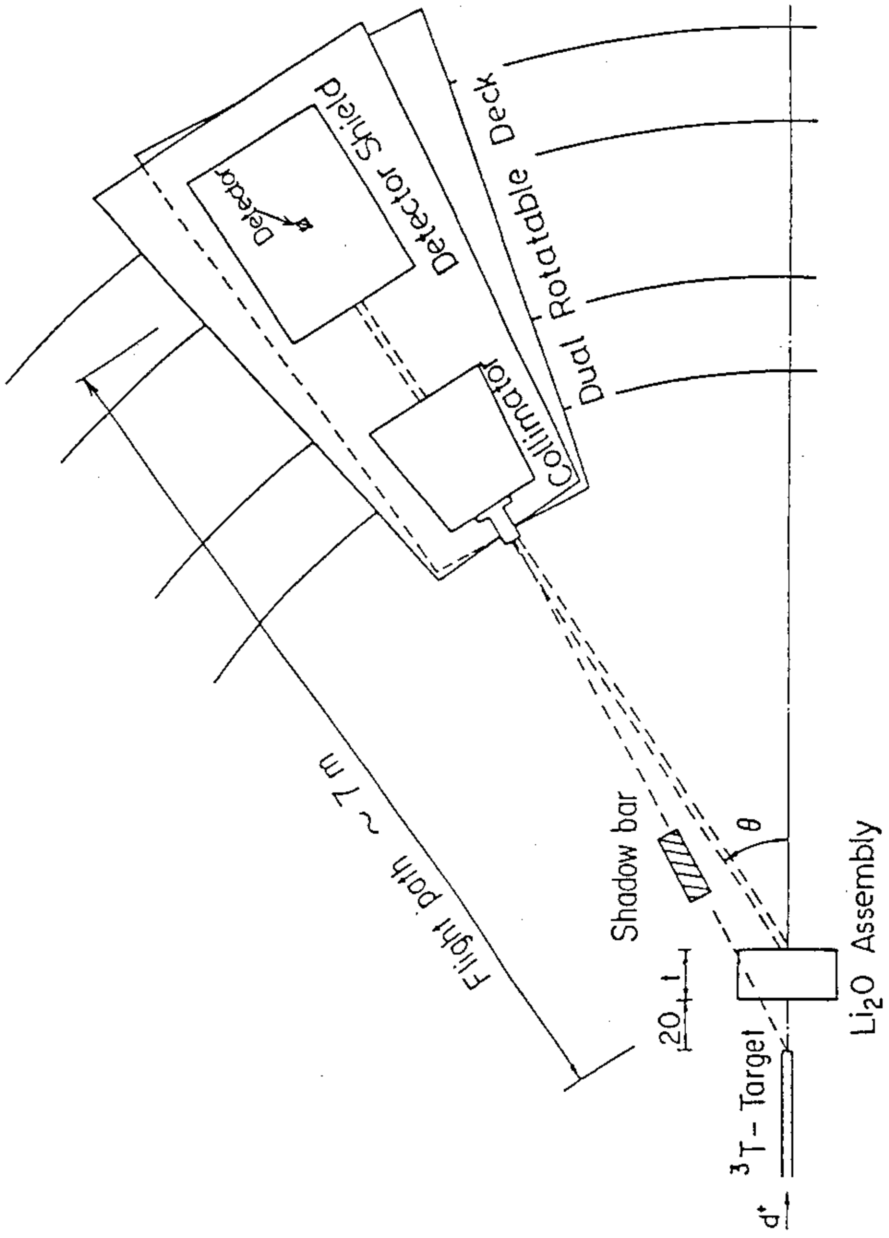

Fig.2.1 Experimental configuration

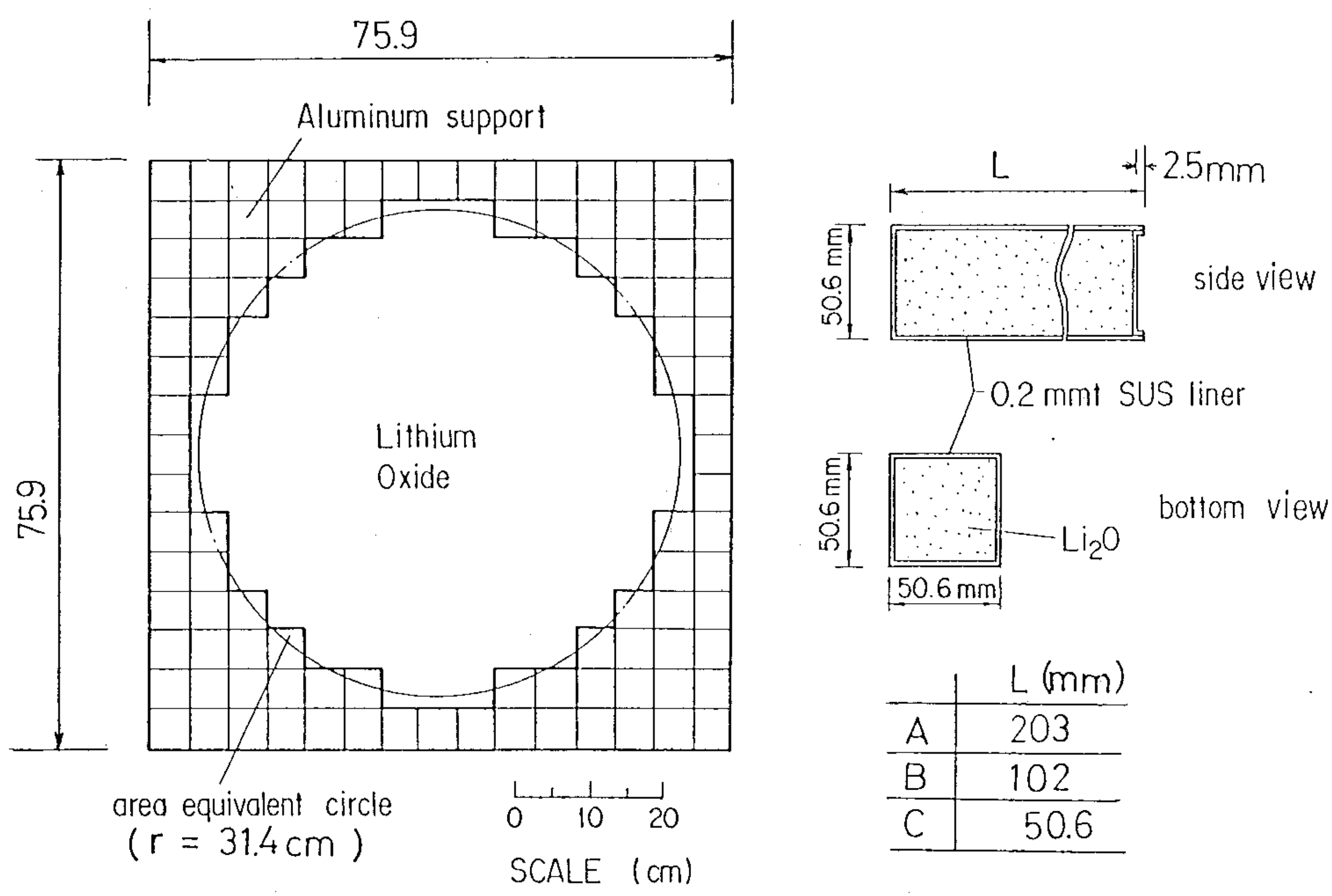

Fig.2.2 Experimental assembly and Li_2O block

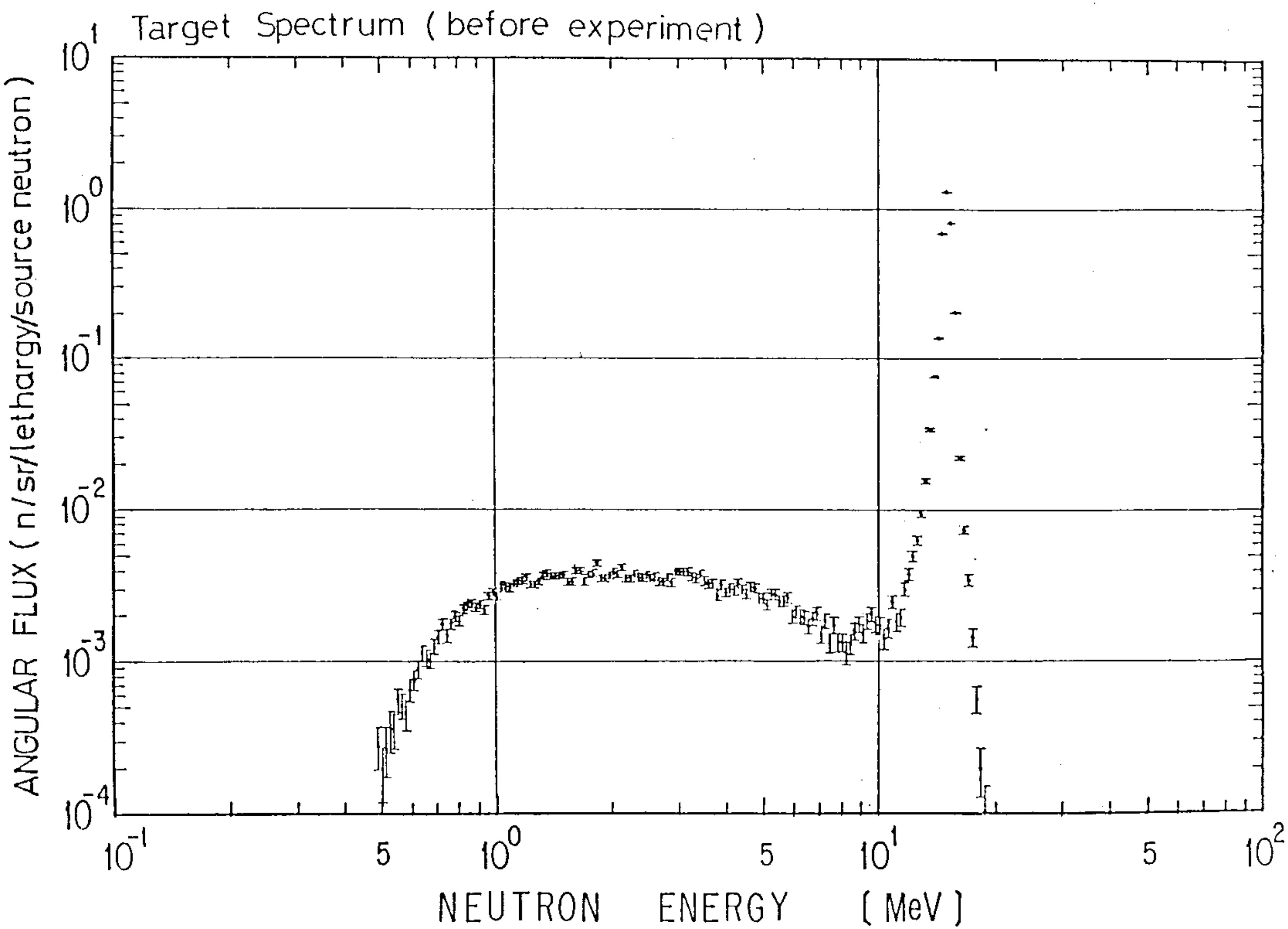

Fig.2.3 Measured neutron spectrum from target assembly to zero-degree direction before the experiment

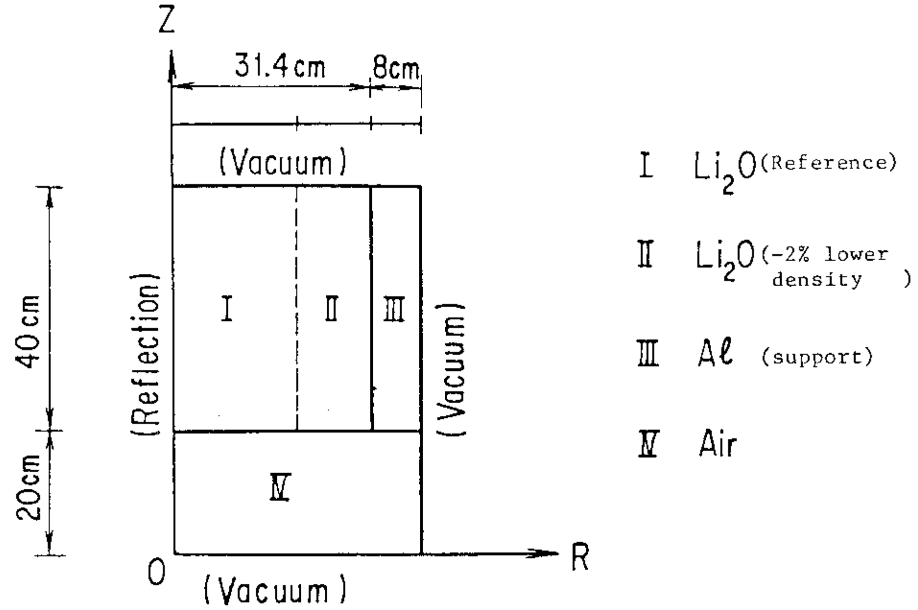

Fig.3.1 Multi-regional model for testing the uncertainty due to the calculational model

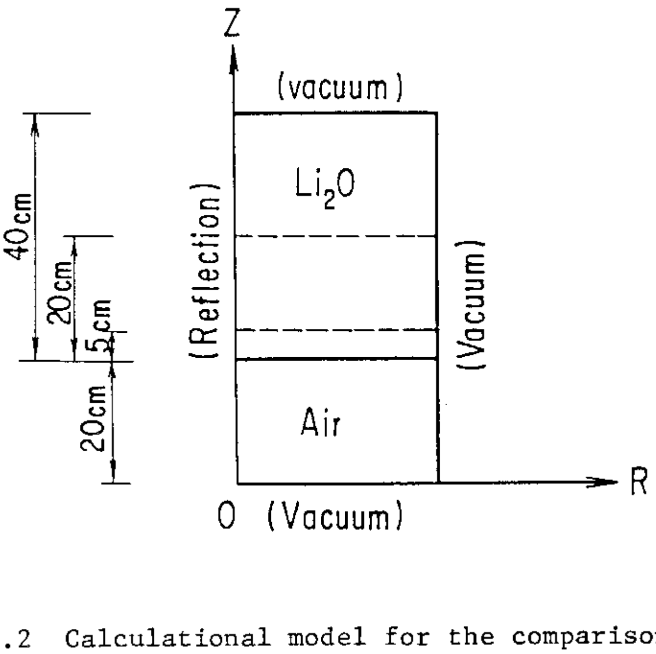

Fig.3.2 Calculational model for the comparison with the experiment

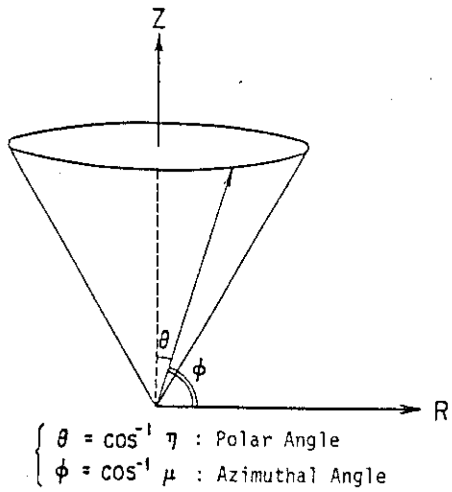

Fig.3.3 Definition of η, μ angles in DOT3.5 calculation

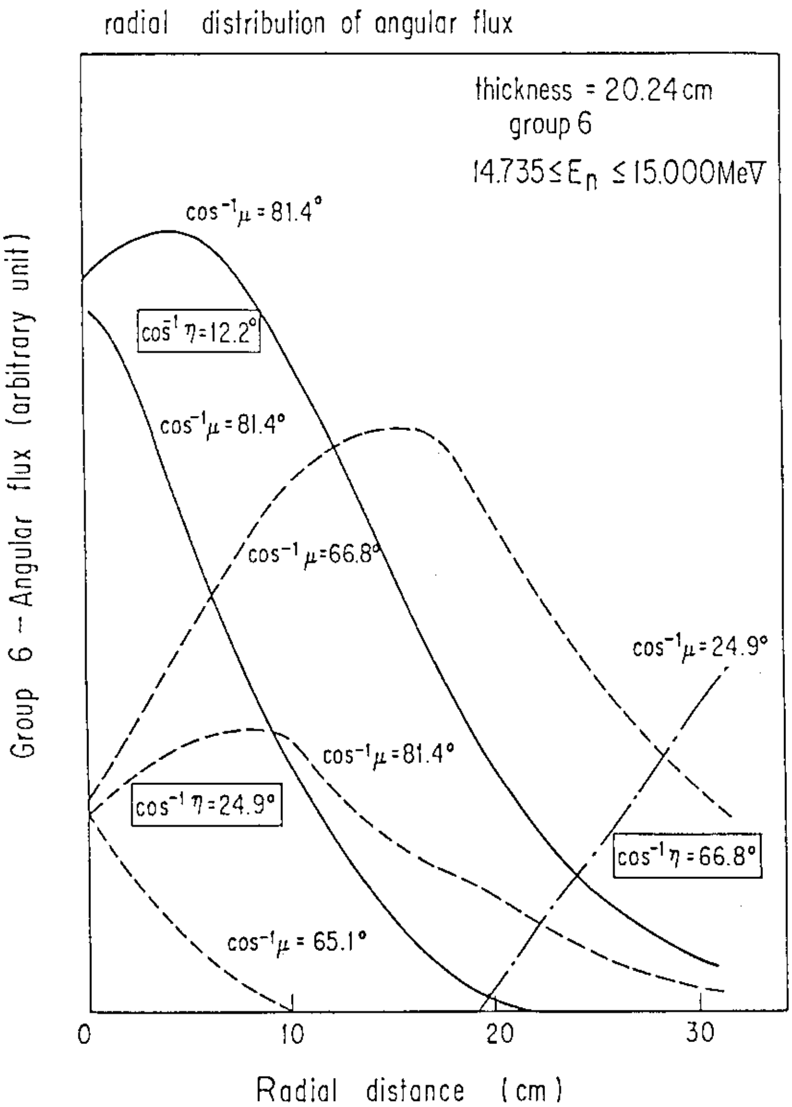

Fig.3.4 Radial distribution of angular flux at typical polar angle $\cos^{-1}\eta$ and azimuthal angle $\cos^{-1}\mu$ on the rear surface of assembly

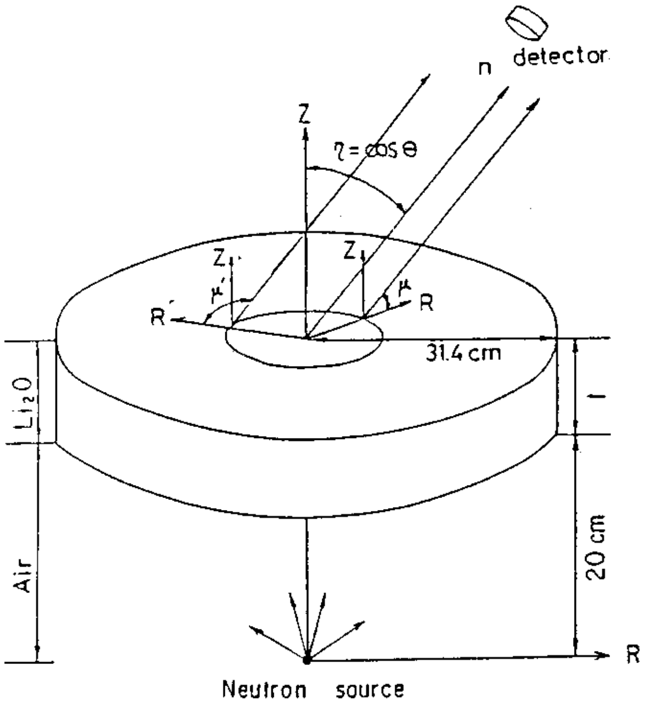

$$\langle\phi\rangle_\mu = \frac{\sum^{\mu} \phi(\eta,\mu)\omega_\mu}{\sum^{\mu} \omega_\mu}$$

$$\langle\phi\rangle_{\mu\cdot R} = \frac{\sum^{r} \langle\phi\rangle_r 2\pi r \Delta r}{\sum^{r} 2\pi r \Delta r}$$

Fig.3.5 The procedure of averaging the angular flux

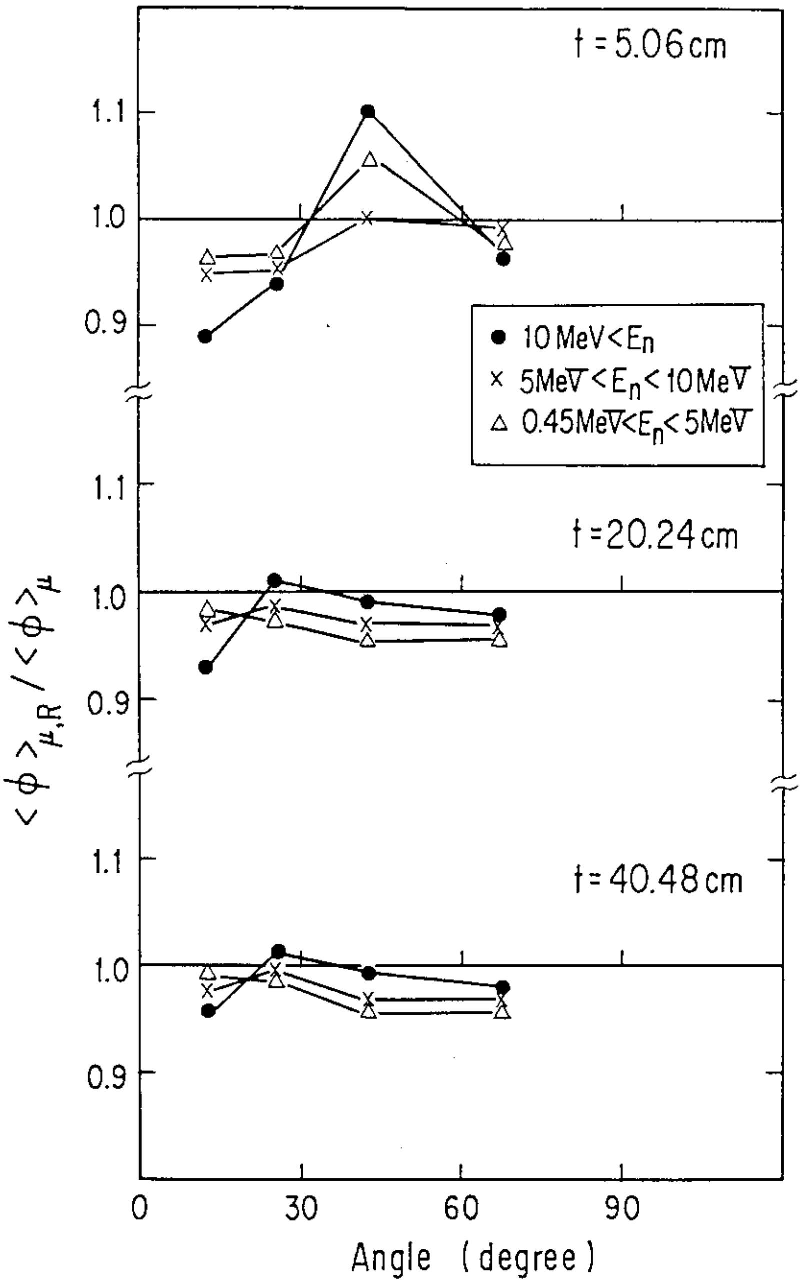

Fig.3.6 Effect of averaging over the measured area (r=0-5 cm)

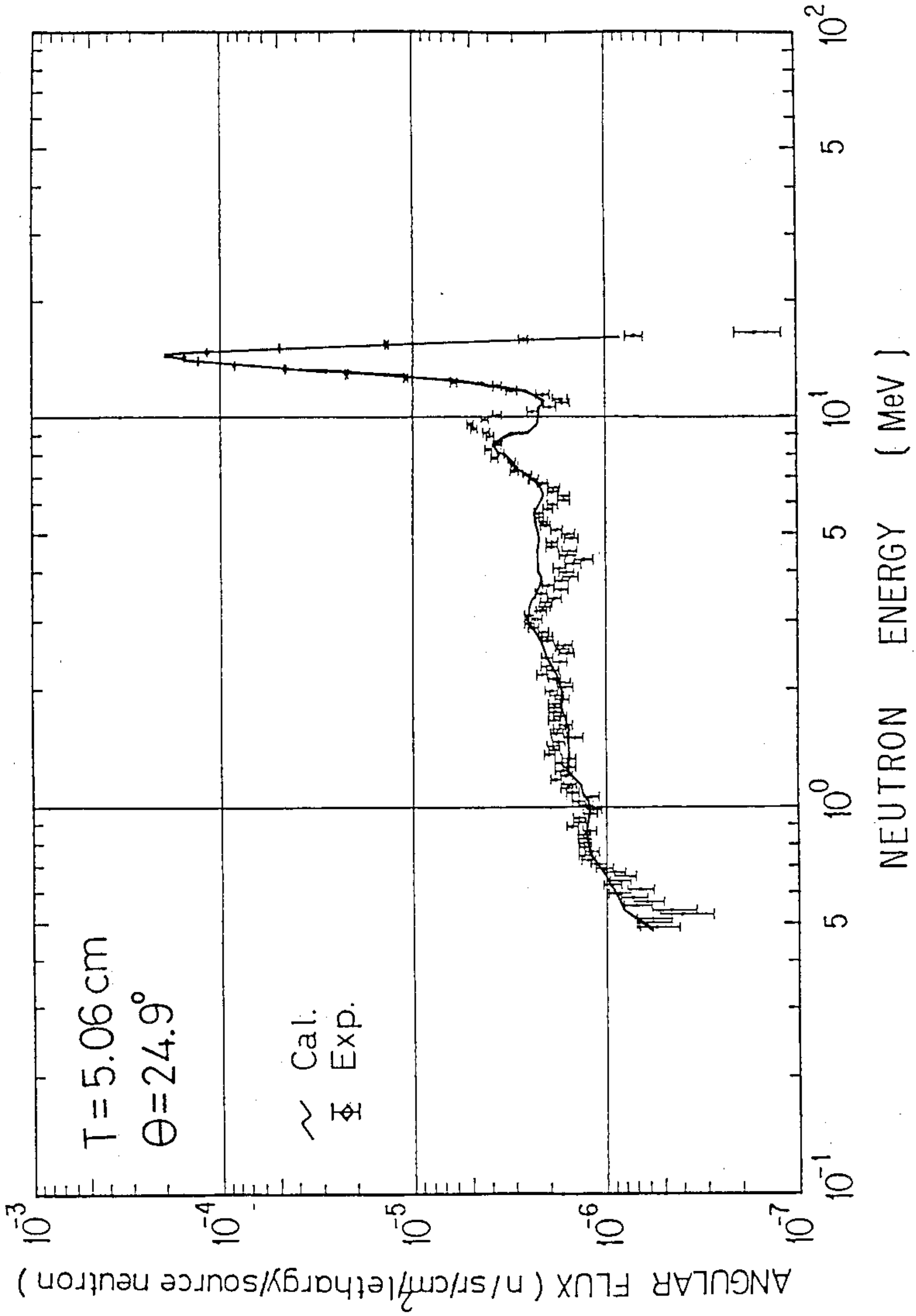

Fig.4.1 Comparison with the experiment (thickness=5.06 cm, angle=24.9 degree)

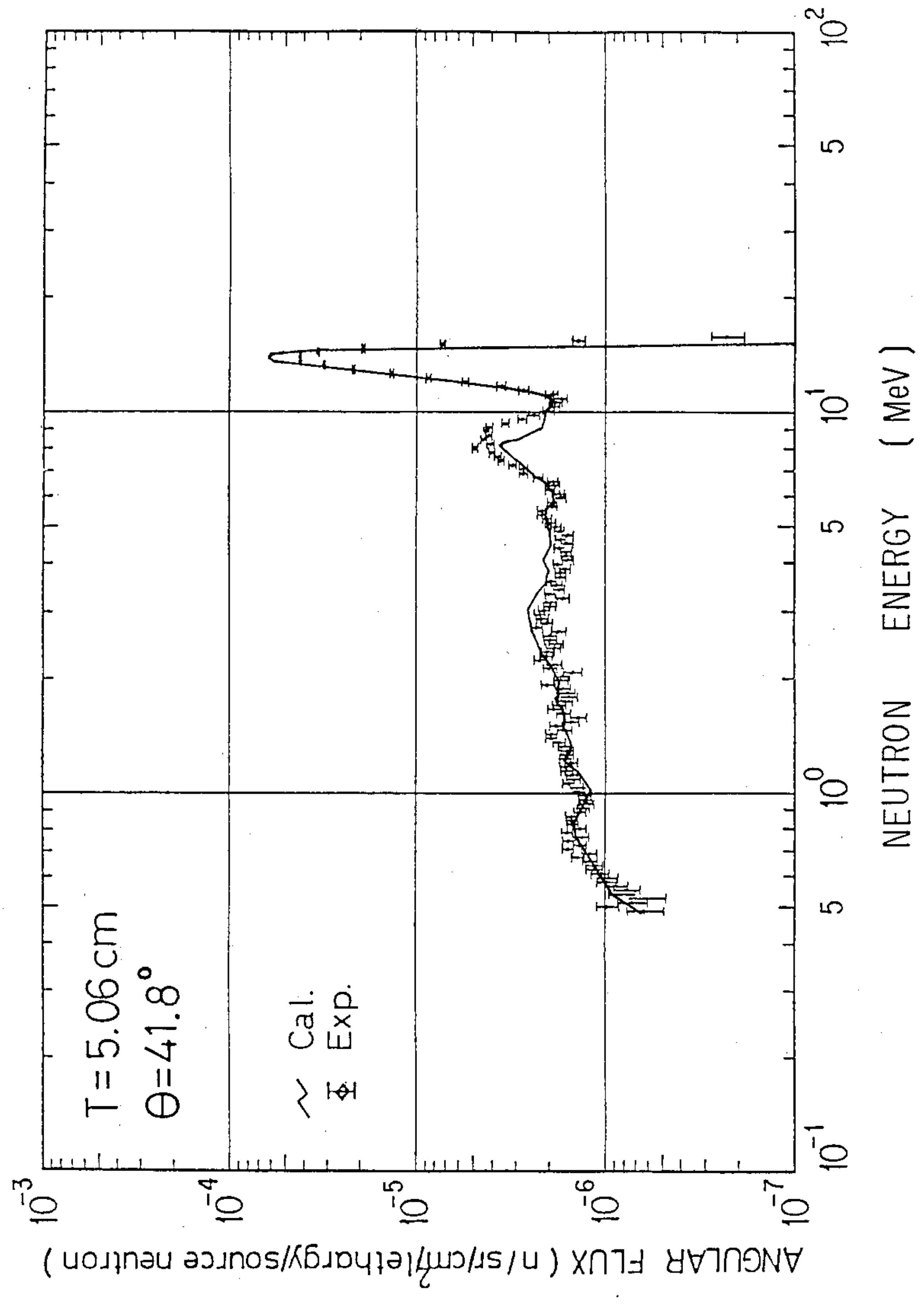

Fig.4.2 Comparison with the experiment (thickness=5.06 cm, angle=41.8 degree)

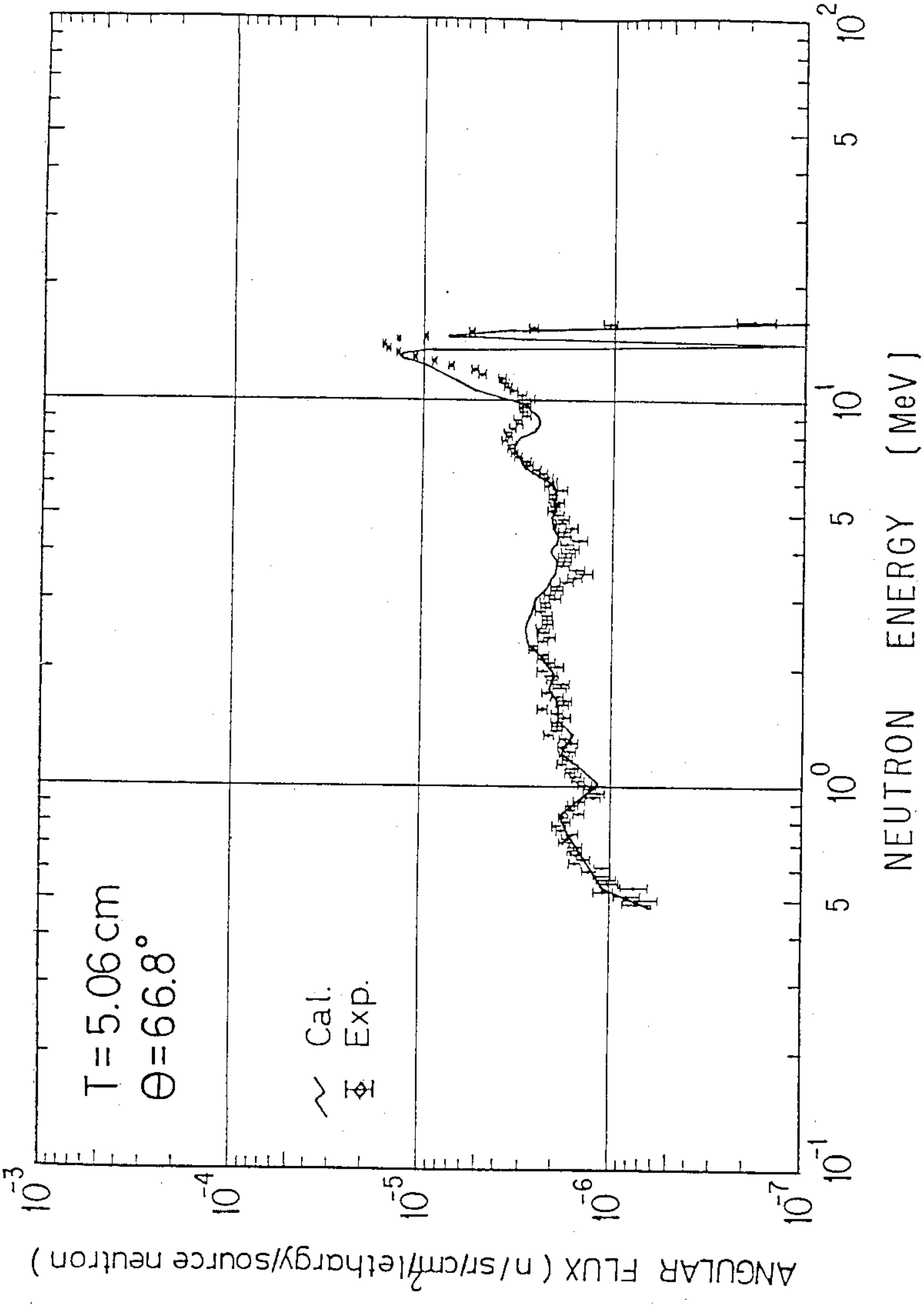

Fig.4.3 Comparison with the experiment (thickness=5.06 cm, angle=66.8 degree)

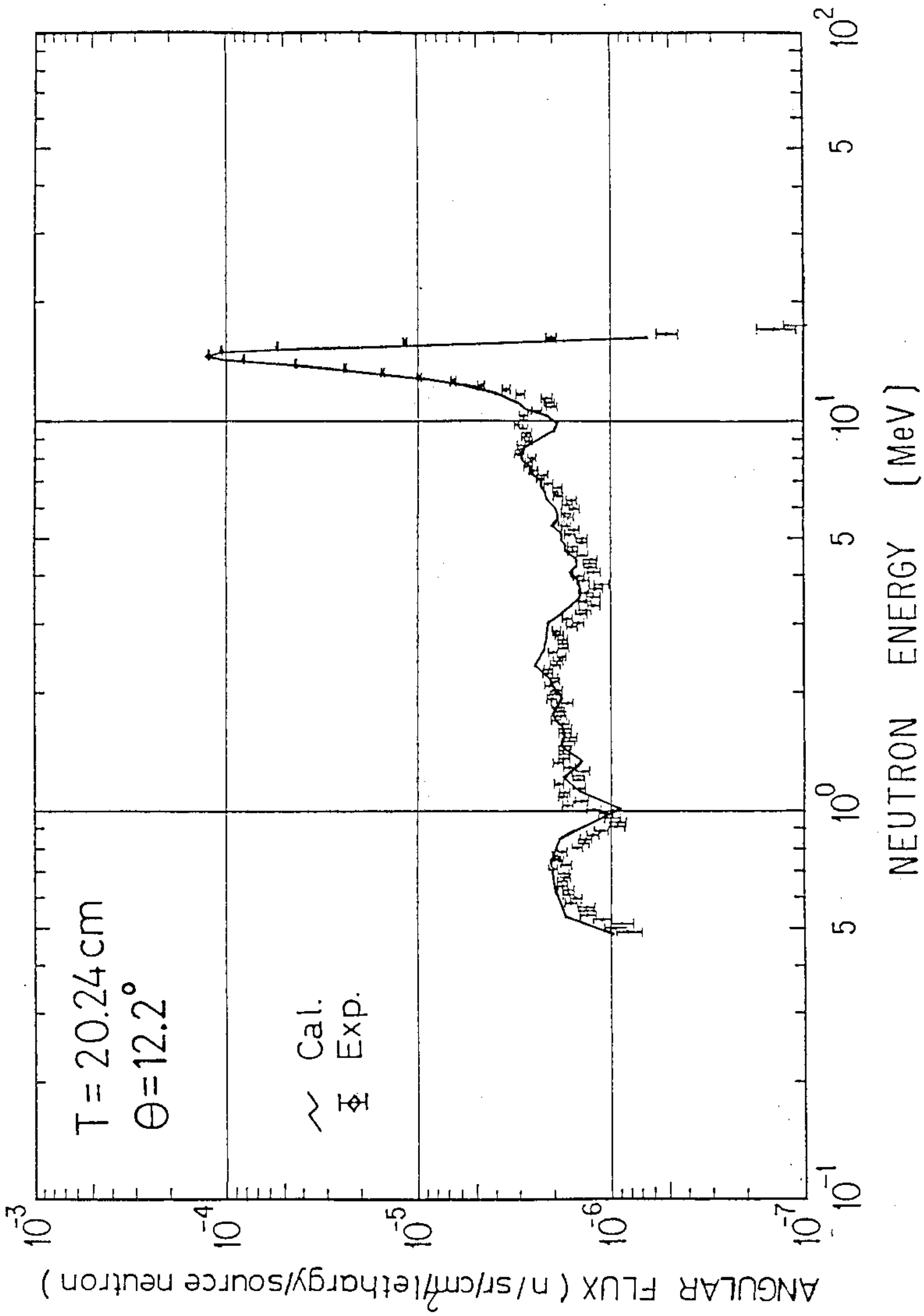

Fig.4.4 Comparison with the experiment (thickness=20.24 cm, angle=12.2 degree)

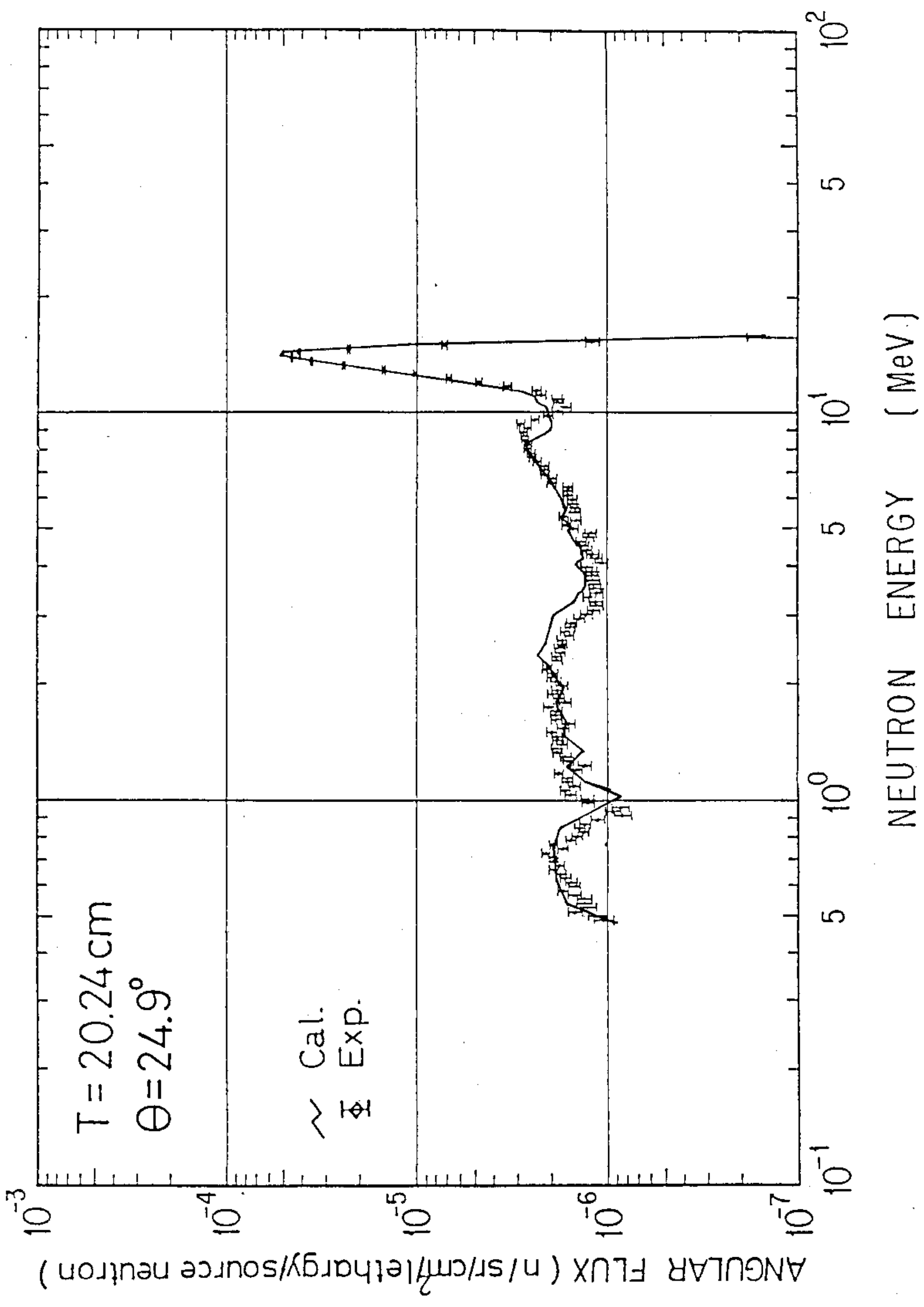

Fig.4.5 Comparison with the experiment (thickness=20.24 cm, angle=24.9 degree)

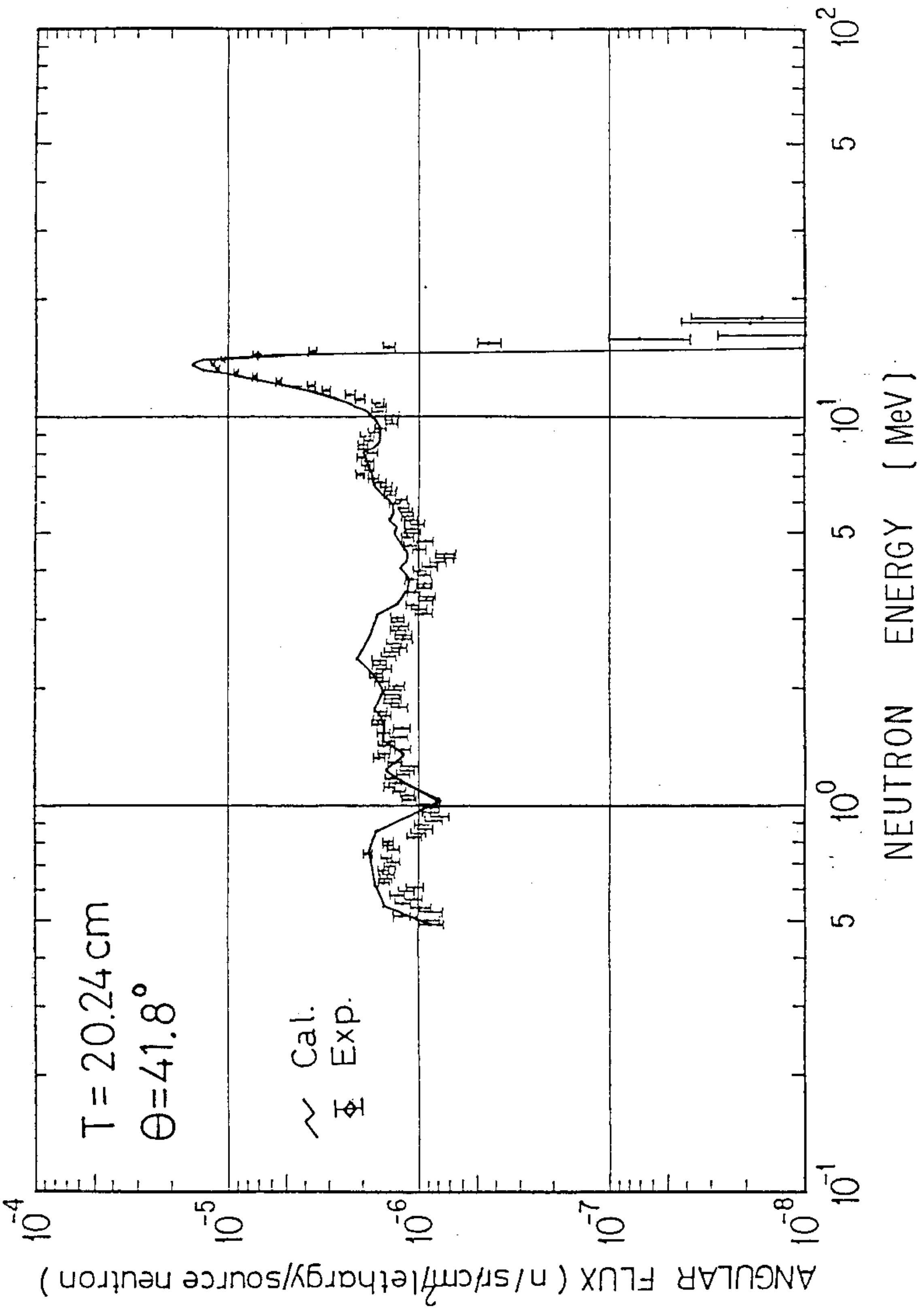

Fig.4.6 Comparison with the experiment (thickness=20.24 cm, angle=41.8 degree)

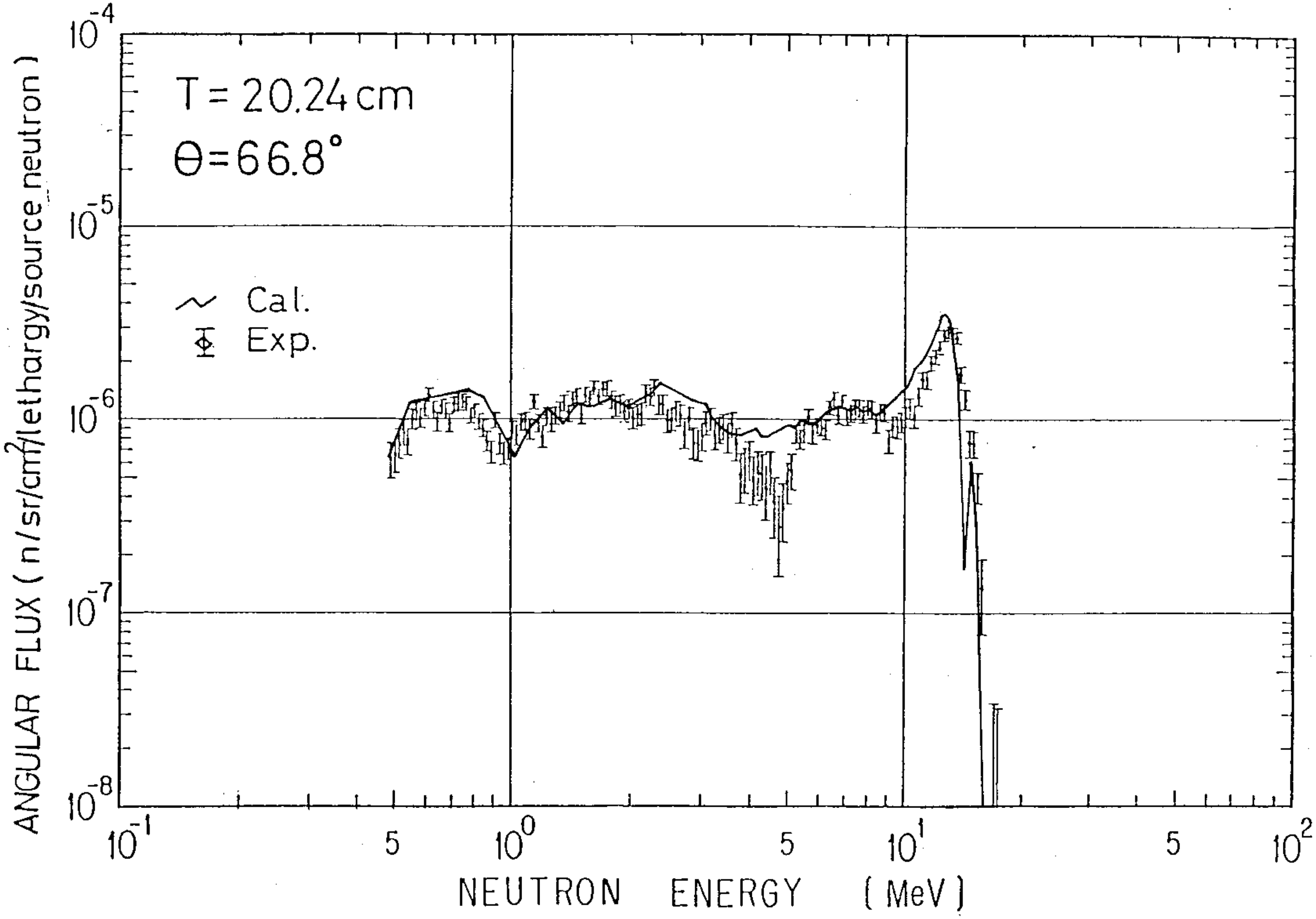

Fig.4.7 Comparison with the experiment (thickness=20.24 cm, angle=66.8 degree)

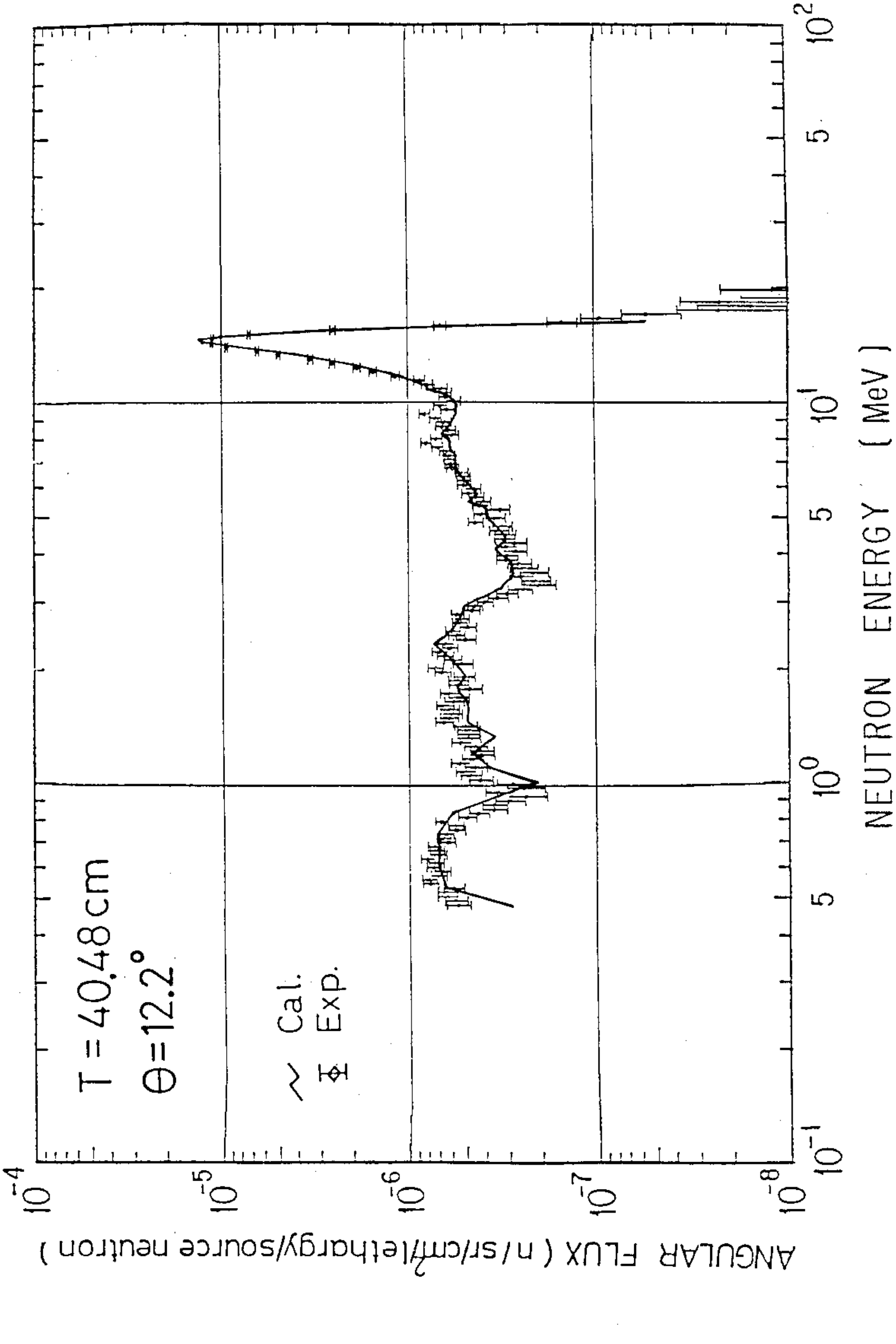

Fig.4.8 Comparison with the experiment (thickness=40.48 cm, angle=12.2 degree)

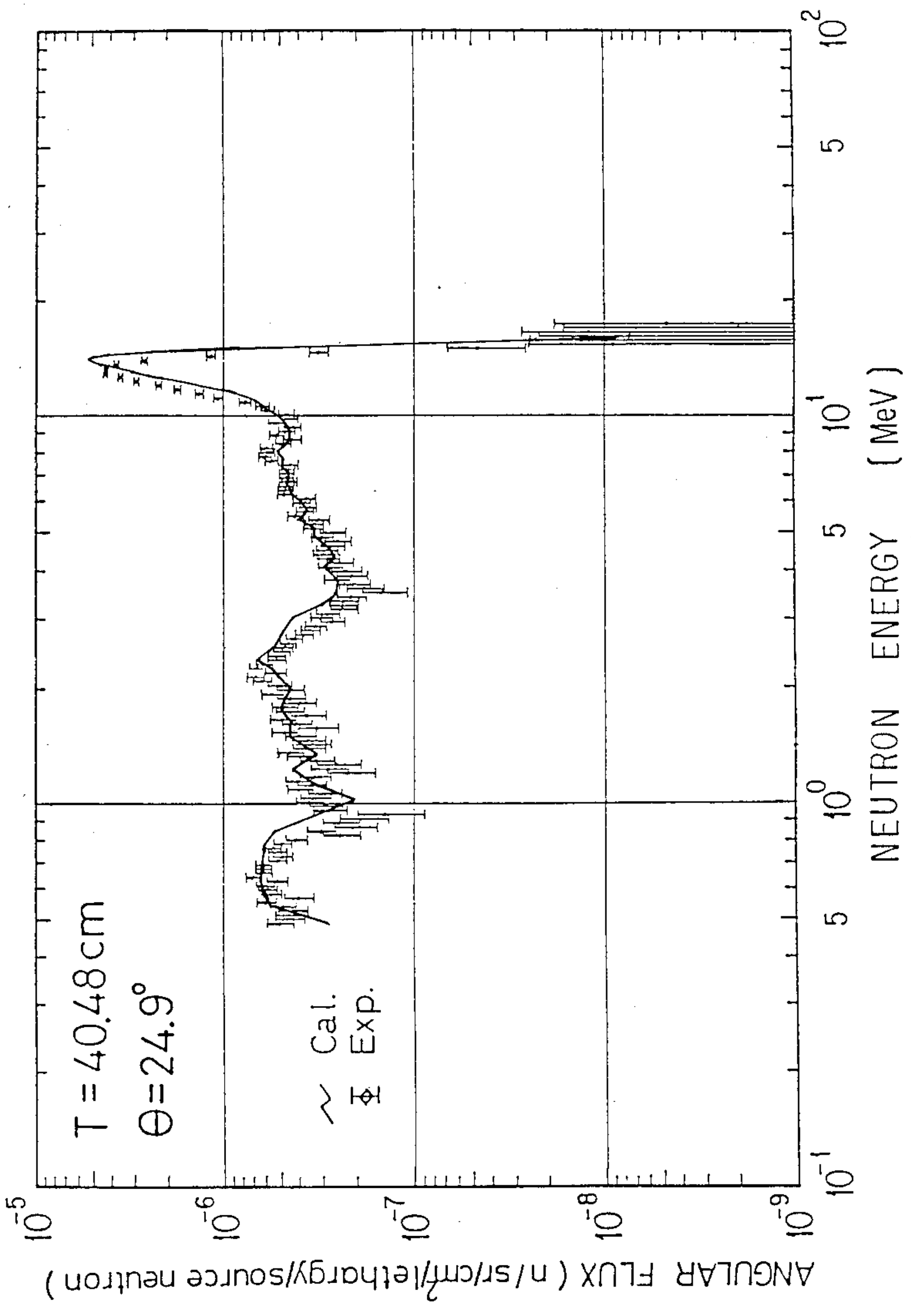

Fig.4.9 Comparison with the experiment (thickness=40.48 cm, angle=24.9 degree)

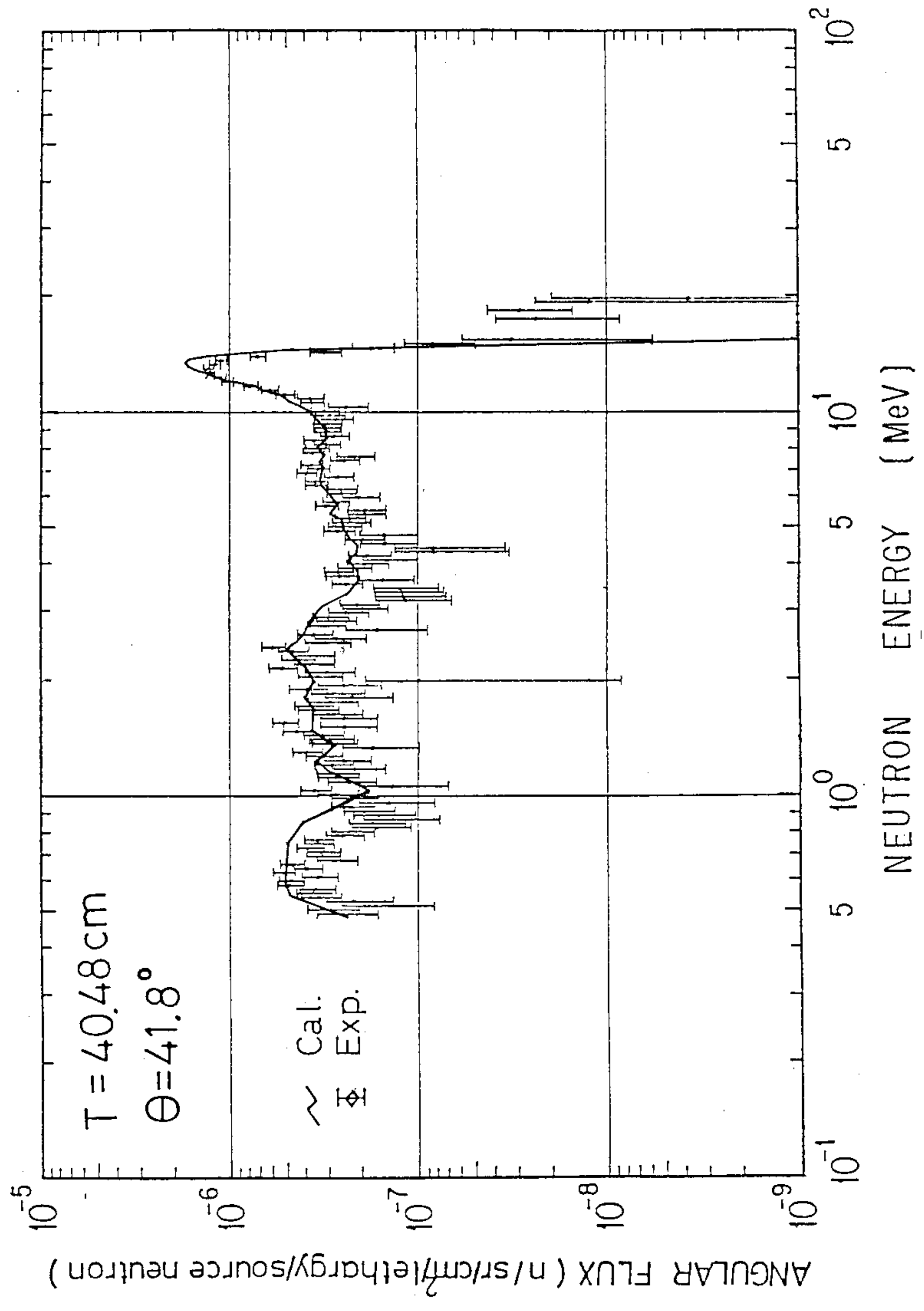

Fig.4.10 Comparison with the experiment (thickness=40.48 cm, angle=41.8 degree)

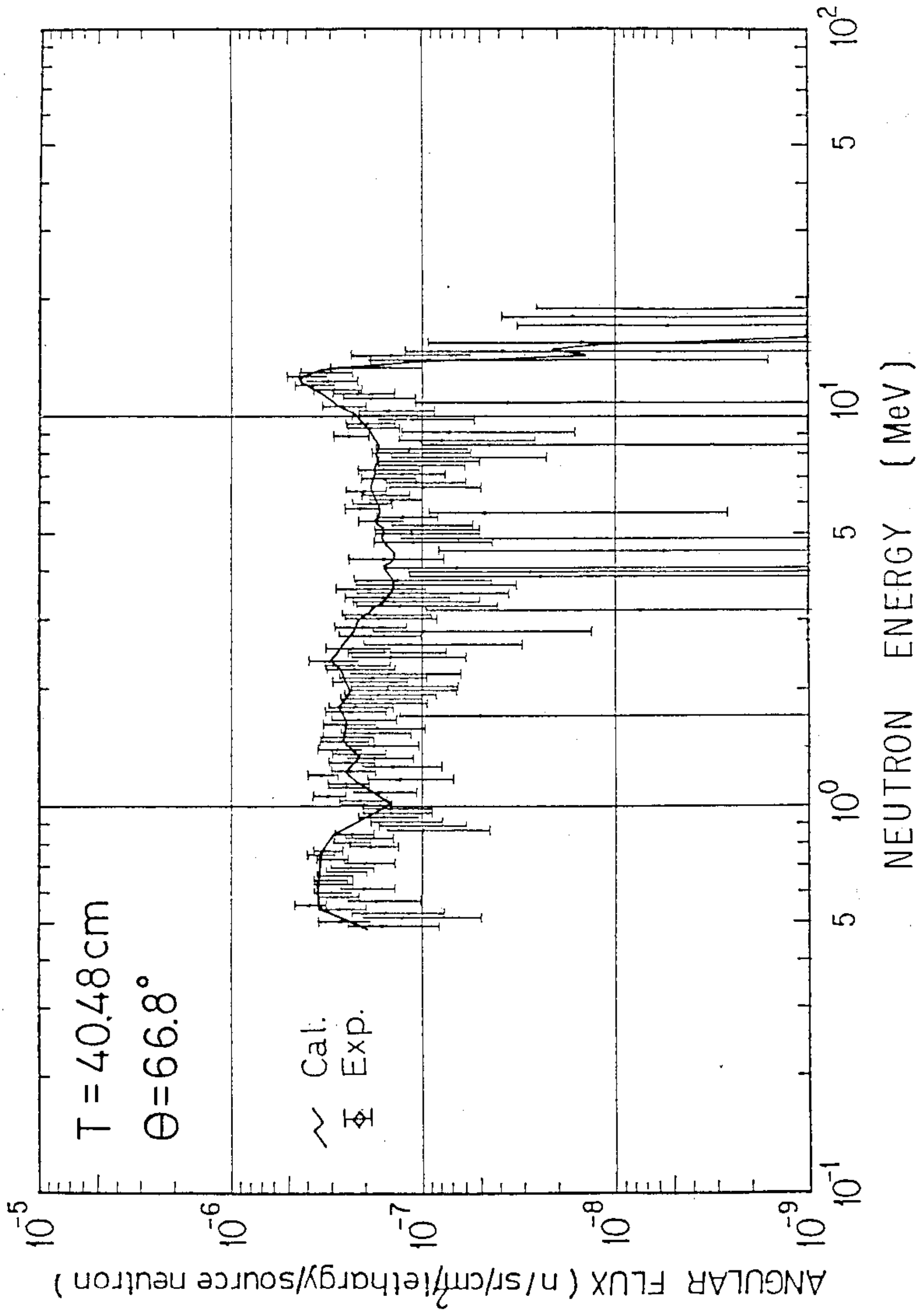

Fig.4.11 Comparison with the experiment (thickness=40.48 cm, angle=66.8 degree)

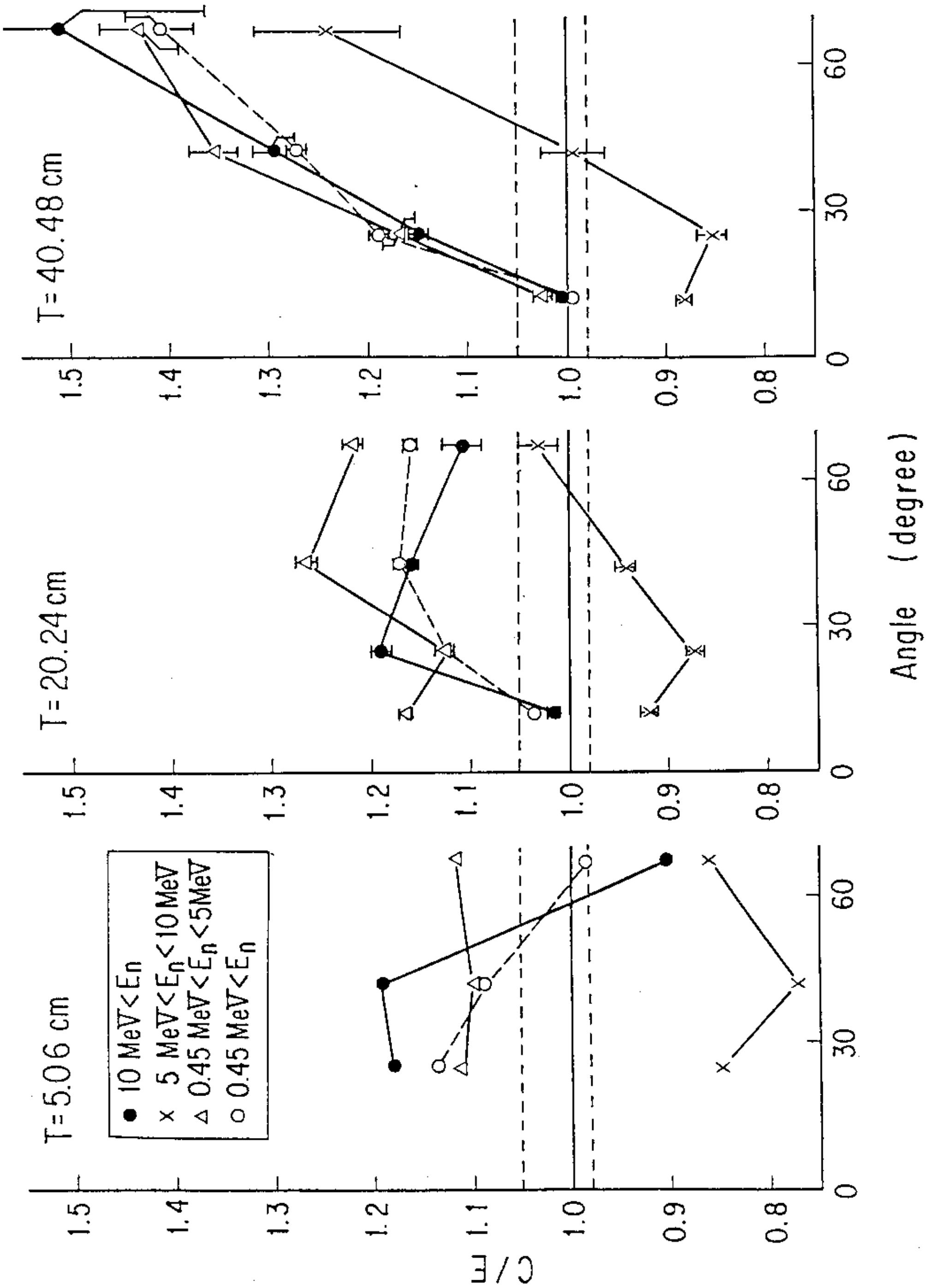

Fig.4.12 Comparison of the integrated fluxes in C/E ratio

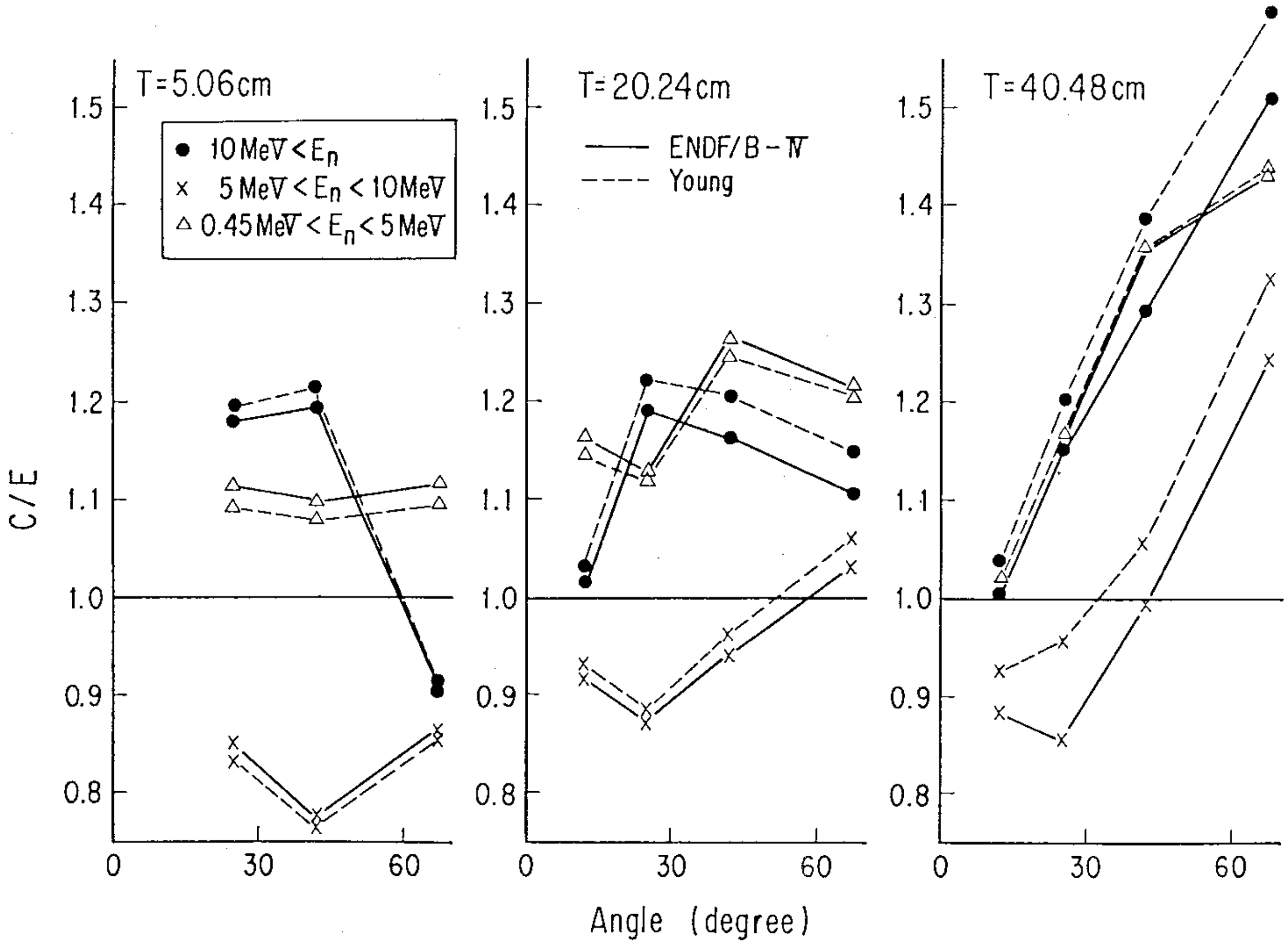

Fig.4.13 Comparison between the integrated fluxes calculated by ENDF/B-4 and by P.G. Young's evaluation of $^7Li(n,n't)^4He$